

Upconversion luminescence of CsScF₄ crystals doped with erbium and ytterbium



D.A. Ikonnikov ^{a,*}, V.N. Voronov ^b, M.S. Molokeev ^{b,c}, A.S. Aleksandrovsky ^{a,b}

^a Siberian Federal University, Krasnoyarsk, Russia

^b L.V. Kirensky Institute of Physics, Krasnoyarsk, Russia

^c Far Eastern State Transport University, Khabarovsk, Russia

ARTICLE INFO

Article history:

Received 25 May 2016

Received in revised form

27 July 2016

Accepted 6 September 2016

Available online 17 September 2016

Keywords:

Fluoride crystals

Erbium

Ytterbium

Up-conversion

Luminescence

Crystal structure

Power dependence

Pump wavelength dependence

ABSTRACT

Tetragonal CsScF₄ crystals doped with (5 at.%) Er and Er/Yb (0.5 at.%/5 at.%) are grown and their crystal structure is determined to belong to *Pmmn* space group. Er and Yb ions are shown to occupy distorted octahedral Sc sites with the center of inversion. Bright visible upconversion luminescence was observed under 970–980 nm pumping with red (⁴F_{9/2}), yellow (⁴S_{3/2}) and green (²H_{11/2}) bands of comparable intensity. UCL tuning curves maximize at 972 nm (CSF:Er) and at 969.7 nm (CSF:Er,Yb) pumping wavelengths. Different ratios between yellow-green and red luminescence intensities in CSF:Er and CSF:Er, Yb are explained by contribution of cross-relaxation in CSF:Er UCL. UC in CSF:Er is a three stage process while UC in CSF:Er, Yb is a two stage process. The peculiarities of power dependences are explained by the power-dependent repopulation between starting levels of UC.

© 2016 Elsevier B.V. All rights reserved.

1. Introduction

The research of new materials for upconversion (UC) of infrared radiation to the visible is presently attracting considerable attention, due to potential applications in biological imaging, photovoltaics, solid state lasers, etc [1–13]. Oxide-based lattices for upconverting ions typically offer good quality of crystalline structure; however, probabilities of non-radiative transitions in oxides are commonly high, leading to excessive losses of pumping radiation power. E.g., UC study of YAl(BO₃)₄:Tm, Yb crystal [14] revealed temperature increase of the crystal under 980 nm irradiation by several tens of degrees, for the samples with near-optimal Yb concentration of 20 at. % introduced into the lattice. Fluoride host lattices have appropriate thermal, optical and chemical stability and rather low cutoff phonon energies; due to the latter feature, they are commonly recognized to demonstrate reduced non-radiative losses. Among fluorides, hexagonal β -NaYF₄(NYF) lattice is the most efficient one for upconversion with Er/Yb acceptor/

donor ion pair, both in the form of polycrystalline powders [15] and in the form of nanocrystals [16]. UC advantages of NYF arise from its peculiar crystal structure with two independent sites for Er and Yb ions [17]. Recently, series of studies are done on obtaining of UC luminescence in nanocrystals of scandium-containing fluorides [18–22]. Despite rather small ionic radius of Sc with respect to Y (as well as Er, Yb and other rare-earth ions), it was found on the example of Eu ion that rare-earth ions occupy Sc positions [22]. It would be interesting to test crystal structure of UC fluoride host modified with respect to Na_xScF_{3+x}, for instance, by using larger-ionic-radius ion instead of Na. In the present paper we study UC in the bulk crystals of CsScF₄(CSF) doped either by Er self-UC ion or Er/Yb UC pair of ions.

Er³⁺ ion has an absorption band in the area of 980 nm, which lies in one of the areas of efficient generation of semiconductor lasers. At the same time, this ion has an extensive scheme of levels above the energy corresponding to this wavelength. So it is auto-upconversion ion [23–27] if pumped in the spectral range around 980 nm. However, previous studies have shown that the addition of Yb ion allows you to implement upconversion in many materials with rare-earth elements [14]. Yb³⁺ is luminescent by itself in the infrared region only, and upconversion in it is impossible. Since its

* Corresponding author.

E-mail address: ikdis@yandex.ru (D.A. Ikonnikov).

absorption cross-sectional 980 nm in a variety of hosts is usually higher than the Er's one, Yb³⁺ ion efficiently absorbs infrared radiation and transfers the excitation to Er³⁺ higher-lying levels. As a result, Er³⁺ emits in the infrared and visible spectral regions.

2. Experimental

The perovskite-like CSF crystals doped with Er and Yb were obtained by Bridgeman – Stockbarger method at the hot zone temperature 900 °C. The starting materials were CsF, ScF₃, ErF₃ and YbF₃ of spectral purity grade. To obtain self-UC CSF:Er crystals, 5 at.% of Er were added to the starting mixture, while growth of CSF:Er, Yb crystal was performed from the mixture containing 0.5 at. % of Er and 5 at.% of Yb. The growth was performed in evacuated and sealed platinum ampoules. Temperature gradient inside the heater was 30 K/cm, and the pulling rate was 0.8 mm/h. At the temperature of synthesis the CSF crystal belongs to tetragonal symmetry space group *P4/mmm* [28]. Cooling of the sample to the room temperature results in sequential phase transitions which finally lead to orthorhombic crystal structure belonging to *Pmmn* space group. Single crystals obtained inside platinum ampoules had typical size up to 2 mm. They were used for upconversion studies while the samples for XRD study were obtained by grinding the single crystals.

The powder diffraction data of CSF:Er in wide 2θ range of 5–140° for Rietveld analysis were collected at room temperature with a Bruker D8 ADVANCE powder diffractometer (Cu-K_α radiation) and linear VANTEC detector. The step size of 2θ was 0.016°, and the counting time was 1 s per step. Rietveld refinement was performed by using TOPAS 4.2 [29].

UC was excited by wavelength-tunable ATC4000-980 InGaAs laser diode with the spectral width of generated radiation close to 4 nm across the wavelength and power range used in the measurement. Spectral measurements were done using Ocean Optics HR4000 spectrometer. We conducted two measurements with these samples: a) Observation of dependence of the luminescence spectra on the pump wavelength; b) Observation of dependence of the luminescence spectra on the pump power.

3. Results and discussion

3.1. XRD results

All peaks of powder pattern were indexed by orthorhombic cell (*Pmmn*) with parameters close to CSF [28]. Therefore, this crystal structure was taken as starting model for Rietveld refinement. As far as refined value of cell volume of CSF:Er $V = 435.35$ (4) Å (Table 1) is bigger than $V = 433.21$ (4) Å of pure CSF, so Er³⁺ ion with

ion radii IR (Er³⁺, CN = 6) = 0.89 Å [30] should occupy smaller Sc³⁺ site (IR (Sc³⁺, CN = 6) = 0.745 Å) instead of bigger Cs site (IR (Cs⁺, CN = 8) = 1.74 Å). Moreover, Er³⁺ substitution of Cs⁺ should lead to vacancies which are not energetically beneficial. Refinement of Er³⁺ occupation in Sc³⁺ site lead to concentration x (Er³⁺) = 1.7 (2)%. This value is more than twice smaller than expected 5%, but it was shown that refinement of Er³⁺ concentration lead to nonzero value. Final refinement was performed using fixed value of x (Er³⁺) = 5%. Refinement was stable and gives low *R*-factors (Table 1, Fig. 1). Coordinates of atoms and main bond lengths are in Table 2 and Table 3 respectively.

3.2. Dependence of the UC luminescence spectra on the pump wavelength

UC luminescence spectra of CSF:Er and CSF:Er, Yb crystals irradiated by infrared laser contained three luminescence transitions: $^2\text{H}_{11/2} - ^4\text{I}_{15/2}$ (515–535 nm), $^4\text{S}_{3/2} - ^4\text{I}_{15/2}$ (535–565 nm) and $^4\text{F}_{9/2} - ^4\text{I}_{15/2}$ (635–685 nm). Spectra of CSF:Er and CSF:Er, Yb irradiated at different central wavelengths of infrared laser are presented in Fig. 2a and Fig. 2b, correspondingly. The shape of individual bands and the ratio of band intensities are found to be, in general, independent on the excitation wavelength, evidencing that kinetics of excited states is, in the main features, identical in the whole pump wavelength range. However, more detailed insight of the ratio of band intensities can be attained by examining the tuning curves for individual bands. These tuning curves for three UC luminescence bands noted above are presented in Fig. 3. They are formed mainly by the convolution of spectral dependences of Er and Yb ions absorption with the spectra of infrared laser, the latter being the factor contributing to their broadening. In the maxima of the tuning curves, UC luminescence intensity in the sample with 5% Yb was 2.2 times higher for $^4\text{S}_{3/2} - ^4\text{I}_{15/2}$ band, 3.9 times higher for $^2\text{H}_{11/2} - ^4\text{I}_{15/2}$ band and 3.7 times higher for $^4\text{F}_{9/2} - ^4\text{I}_{15/2}$ band, with respect to the sample doped with 5% Er only. While all three tuning curves for CSF:Er show distinct maximum at 972 nm, the tuning curves for CSF:Er, Yb are more broad. Curves for $^4\text{S}_{3/2} - ^4\text{I}_{15/2}$ and $^4\text{F}_{9/2} - ^4\text{I}_{15/2}$ bands maximize at the boundary of infrared laser tuning range 969.7 nm, actual maximum being expected below this value. Tuning curve for $^2\text{H}_{11/2} - ^4\text{I}_{15/2}$ band maximizes at 973 nm, while additional shorter-wavelength maximum can be suspected but not strictly judged from available data. Normalized difference curves between tuning curves of CSF:Er, Yb and CSF:Er (Fig. 4) were obtained by subtraction of CSF:Er tuning curves divided by 10 from of

Table 1
Main parameters of processing and refinement of the CSF:Er.

Compound	CSF:Er
Sp.Gr.	<i>Pmmn</i>
<i>a</i> , Å	8.0036 (4)
<i>b</i> , Å	7.9930 (6)
<i>c</i> , Å	6.8053 (3)
<i>V</i> , Å ³	435.35 (4)
2θ-interval, °	5–140
No. of reflections	480
No. of refined parameters	67
<i>R</i> _{wp} , %	6.28
<i>R</i> _p , %	4.79
<i>R</i> _{exp} , %	5.00
χ^2	1.26
<i>R</i> _B , %	1.66

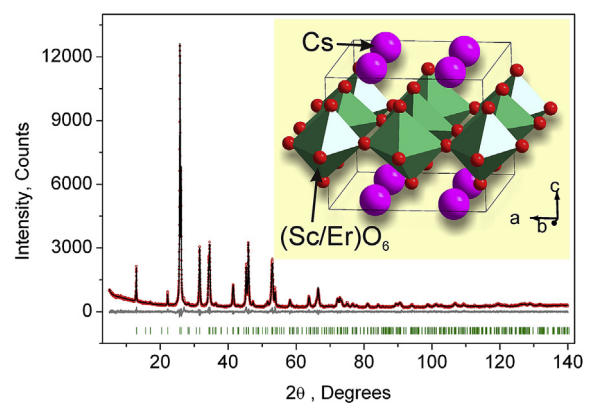


Fig. 1. Difference Rietveld plot of CSF:Er. Inset shows crystal structure. Red points at the graph are experimental points, and black line is the result of Rietveld refinement. Oxygen atoms at the tops of polyhedra are depicted by the red. (For interpretation of the references to colour in this figure legend, the reader is referred to the web version of this article.)

Table 2

Fractional atomic coordinates and isotropic displacement parameters (\AA^2) of CSF:Er.

	x	y	z	B_{iso}	Occ.
Cs1	0.25	0.25	-0.003 (2)	2.4 (2)	1
Cs2	0.25	0.75	-0.0176 (5)	2.4 (2)	1
Sc	0	0	0.5	1.1 (1)	0.95
Er	0	0	0.5	1.1 (1)	0.05
F1	0.25	0.553 (2)	0.481 (4)	2.0 (2)	1
F2	0.001 (3)	0.25	0.463 (2)	2.0 (2)	1
F3	0.468 (1)	0.495 (3)	0.2135 (6)	2.0 (2)	1

Table 3

Main bond lengths (\AA) of CSF:Er.

Cs1—F3	3.01 (2)	(Sc/Er)—F1 ⁱⁱ	2.050 (3)
Cs1—F3 ⁱ	3.36 (2)	(Sc/Er)—F2	2.014 (2)
Cs2—F3	3.11 (2)	(Sc/Er)—F3 ⁱⁱⁱ	1.967 (4)
Cs2—F3 ⁱ	3.27 (2)		

Symmetry codes: (i) -x+1, -y+1, -z; (ii) -x, y-1/2, -z+1; (iii) -x+1/2, -y+1/2, z.

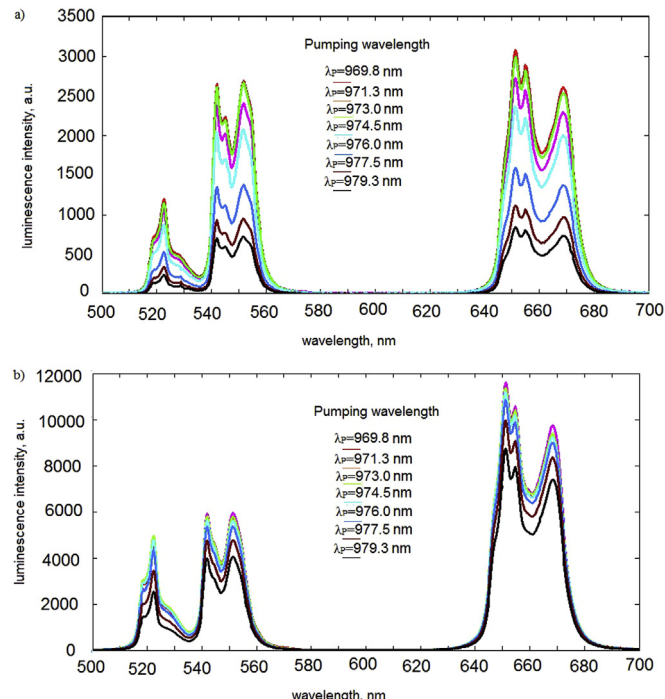


Fig. 2. UC luminescence spectra of CSF:Er (a) and CSF:ErYb (b) irradiated at different central wavelengths of infrared laser.

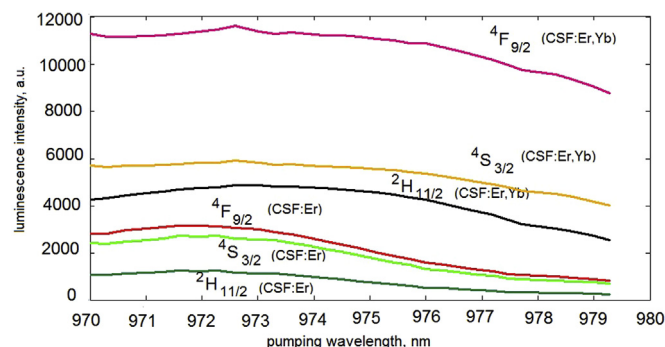


Fig. 3. Tuning curves for three UC luminescence bands.

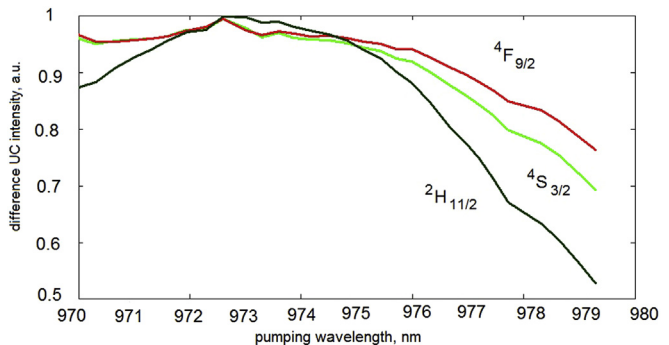


Fig. 4. Normalized difference curve between tuning curves of CSF:Er, Yb and CSF:Er upconversion luminescence.

CSF:Er, Yb tuning curves. The pump wavelength dependence in Fig. 4 is due to variation of the detuning from nearest Er and Yb levels, while the difference between tuning curve behavior for different UCL lines is due features of population routes, as discussed below. These difference curves reveal presence of two maxima, namely, maximum at 973 nm and possible maximum at 969 nm or below. This feature must be ascribed to spectral dependence of Yb absorption in CSF lattice. The presence of multicomponent absorption spectrum of Yb ions within the spectral region of interest can be found in a number of papers, e.g., in Ref. [31] for YbAB crystal and in Ref. [32] for Yb elpasolite, though shift of peaks and redistribution of their intensities may be expected in CSF matrix with respect to other ones. Suggestively, Yb absorption peaks detected in UC luminescence can be ascribed to pure electronic transitions ${}^2F_{7/2}$ / ${}^2G_6 \rightarrow {}^2F_{5/2}$ / 2G_8 (below 969 nm) of Yb ion in octahedral coordination and its vibronic satellite (973 nm).

Comparing UC luminescence of samples CSF:Er and CSF:Er,Yb, we see that there is enhancement of UC signal in CSF:Er, Yb sample as compared with CSF:Er, like it was established in a number of other hosts, due to larger Yb absorption of pump radiation with respect to Er at the same concentration. However, enhancement of red (${}^4F_{9/2} - {}^4I_{15/2}$) and green (${}^2H_{11/2} - {}^4I_{15/2}$) luminescence in Yb-containing crystal is more strong than enhancement of green-yellow luminescence (${}^4S_{3/2} - {}^4I_{15/2}$). Explanation of this feature is connected with different concentration of Er in these samples and therefore, different rate of cross-relaxation. Namely, due to higher concentration of Er in CSF:Er sample, the cross-relaxation on the ${}^2G_{9/2} \rightarrow {}^4S_{3/2}$ (6374 el paso) transition with simultaneous excitation on ${}^4I_{15/2} \rightarrow {}^4I_{13/2}$ (6346 el paso) transition is the additional pathway for population of starting state of green-yellow luminescence, that is absent in Yb-doped sample with its low Er concentration. This mechanism is supported by the fact that luminescence from ${}^2G_{9/2}$ state (405 nm) in pure Er sample is 10 times smaller than in Yb, Er sample.

3.3. Dependence of the luminescence spectra on the pump power

Measurements of UC power dependence were done at constant central wavelength 969.7 nm that is close to tuning curves' maxima both for CSF:Er and CSF:Er, Yb samples. Infrared laser power on the samples varied in the range from 45 to 100 mW, which corresponded to the intensity in the range 1.4–3.2 W/cm². Spectra UC luminescence at different pump powers are presented in Fig. 5a for CSF:Er and in Fig. 5b for CSF:Er,Yb. The shape of individual bands and the ratio of the bands in every sample are preserved over all the range of power variation, indicating again that population kinetics is not changing both in tuning the pump wavelength and pump power. The log-to-log dependencies of integrated UC luminescence

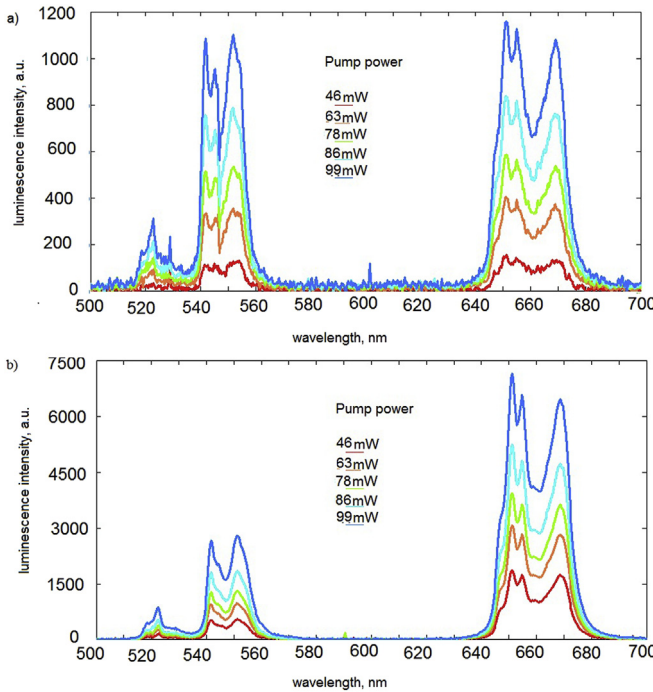


Fig. 5. Spectra of UC luminescence at different pump powers (in the range 46–99 mW) for CSF:Er (a) and CSF:Er, Yb (b).

on the pump power for three bands are presented in Fig. 6. For CSF:Er sample we observe $I_{UC} = P^n$ with $2 < n < 3$ for different bands that indicates that population of starting levels of UCL is dominated by a three-stage process. Typically for self-upconversion in Er ion level system under pumping through $^4I_{11/2}$ level at Er content of order of 2–5% two-stage UC process is dominating for red, green and green-yellow lines [25–27], enabling $1.5 < n < 2$ or slightly higher than 2. Three-stage process for (Er $^4I_{11/2}$) was observed rarely, for instance in Ref. [26] for 1.8 at.% of Er. The n value around 2.9 for yellow-green and green bands in CSF:Er sample could be explained by cascade excitation (arrows indicate GSA and ETU, waves indicate radiativeless relaxation): $^4I_{15/2} \rightarrow ^4I_{11/2} \sim ^4I_{13/2} \rightarrow ^4F_{9/2} \sim ^4I_{9/2} \rightarrow ^4F_{5/2}$ or $^4I_{15/2} \rightarrow ^4I_{11/2} \sim ^4I_{13/2} \rightarrow ^4F_{9/2} \rightarrow ^2G_{9/2}$ if radiativeless relaxation from $^4F_{5/2}$ or $^2G_{9/2}$ to $^2H_{11/2}/^4S_{3/2}$ dominates over two-photon excitation $^4I_{15/2} \rightarrow ^4I_{11/2} \rightarrow ^4F_{7/2} \sim ^2H_{11/2}/^4S_{3/2}$. Domination may be caused by strong radiativeless relaxation from $^4I_{11/2}$. However, cascade excitation cannot explain $n = 2.7$ for the

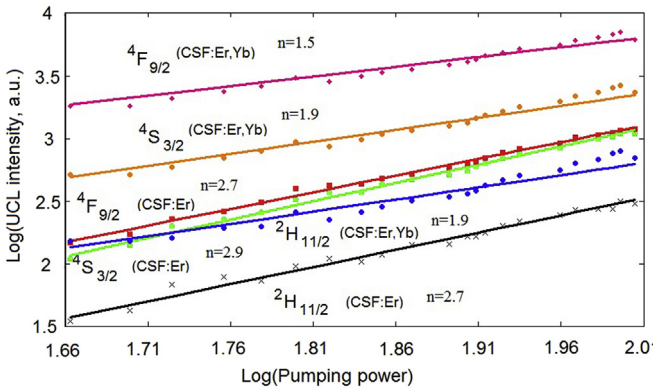


Fig. 6. The log-to-log dependencies of integrated UC luminescence on the pump power for three spectral bands.

red line. This conclusion is in agreement with theoretical consideration in Ref. [33] who established that n for red band in self-upconversion using Er ion could not be above 2 for both ETU and ESA processes. Therefore, the only mechanism explaining observed n for all bands is cross-relaxation process. Three possible CR channels can be found in the Er energy scheme (Fig. 7) $^2G_{9/2} \rightarrow ^4S_{3/2} = ^4I_{9/2} \rightarrow ^4S_{3/2}$ (estimated detuning in a fluoride crystal 295 cm^{-1}), $^4F_{5/2} \rightarrow ^4S_{3/2} = ^4F_{9/2} \rightarrow ^2H_{11/2}$ (detuning 71 cm^{-1}) and $^2G_{9/2} \rightarrow ^4S_{3/2} = ^4I_{15/2} \rightarrow ^4I_{13/2}$ (detuning 28 cm^{-1}). The latter channel is the most probable in view of smallest detuning. The suggestion that $G_{9/2}$ level is involved into the UC excitation processes is supported by the fact that we observed rather weak luminescence from this level to the ground state, as already discussed in the subsection on UC wavelength dependence. The power dependence for this violet line is 2.9, in agreement with suggested UC process mechanism.

For CSF:ErYb sample we observe $1.5 < n < 2$ for different bands, that indicates that population of starting levels of UCL is dominated by a two-stage process (Fig. 8). We have much smaller concentration of Er^{3+} ion in this sample with respect to our previously described self-converting sample, therefore, the probabilities of cross-relaxations are expected to be much smaller, too. Excitation of red and yellow-green/green luminescence starting levels are expected to be $^4I_{15/2} \rightarrow ^4I_{11/2} \sim ^4I_{13/2} \rightarrow ^4F_{9/2}$ or $^4I_{15/2} \rightarrow ^4I_{11/2} \rightarrow ^4F_{7/2} \sim ^2H_{11/2}/^4S_{3/2} \sim ^4F_{9/2}$ and $^4I_{15/2} \rightarrow ^4I_{11/2} \rightarrow ^4F_{7/2} \sim ^2H_{11/2}/^4S_{3/2}$ respectively, but n value for red line is only 1.5 while n for yellow-green/green lines is 1.9. However, according to treatment of Pollnau et al. [33], the conditions for UC excitation for both red and yellow green band are equivalent. Therefore, power dependence must be equal for both of UC bands, and some additional mechanism of population/depopulation must be taken into account to explain the observed difference. This difference must be caused by contribution of depopulation pathway from level $^4F_{9/2}$ to $^2G_{9/2}$ with the subsequent decay $^2G_{9/2} \sim ^2H_{11/2}/^4S_{3/2}$. Under weak infrared pumping, ETU from $^4F_{9/2}$ to $^2G_{9/2}$ is negligible due to small populations at Yb $^4F_{5/2}$

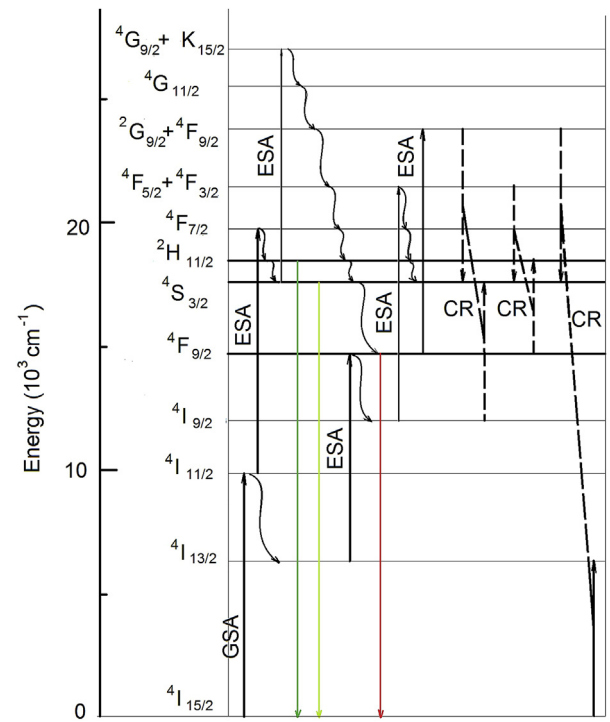


Fig. 7. The scheme of Er ion energy levels and UC-related transitions for self-UC process in CSF:Er.

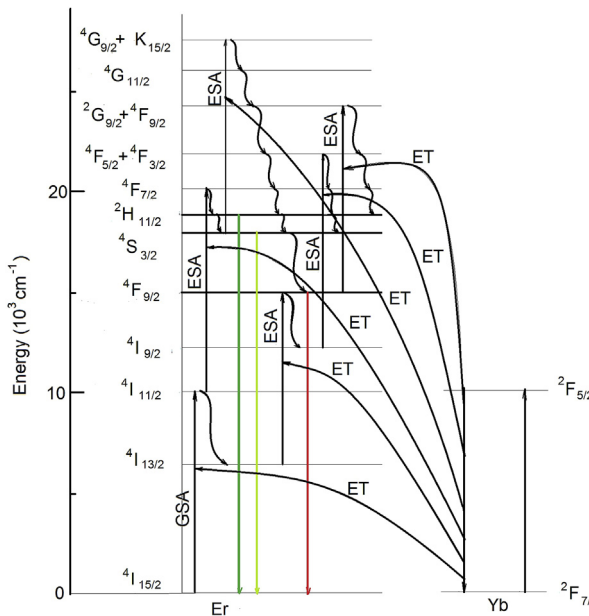


Fig. 8. The scheme of energy levels and UC-related transitions for UC process in CSF:Er,Yb.

and Er ${}^4F_{9/2}$, and n approx 2 for all bands. At sufficient pump power the redistribution channel noted above becomes important, and the difference between red and yellow/green UC power dependencies establishes. Within rather narrow power range available for our measurements this mechanism results in observed difference of power dependences.

4. Conclusion

Tetragonal CSF crystals doped with (5 at.%) Er or Er/Yb (0.5 at.%) are grown using Bridgeman – Stockbarger method. Crystal structure is determined to belong to $Pmmn$ space group. Er and Yb ions are shown to occupy distorted octahedral Sc sites. Despite presence of center of inversion, bright visible upconversion luminescence with red (${}^4F_{9/2}$), yellow (${}^4S_{3/2}$) and green (${}^2H_{11/2}$) bands of comparable intensity was observed under 970–980 nm pumping. UCL tuning curve in CSF:Er maximizes at 972 nm pumping wavelength, while tuning curves for CSF:Er, Yb are more broad and maximize at the boundary of infrared laser tuning range 969.7 nm. UC in CSF:Er is a three stage process for all three mentioned bands; the log-to-log slope of UCL dependence on the pump power is 2.7 for red, 2.9 for yellow and 2.7 for green band. Observed peculiarities of this dependence for different bands are explained by presence of cross-relaxation. Contribution of cross-relaxation also explains different ratio between yellow and red luminescence intensities in CSF:Er and CSF:Er,Yb. UC in CSF:Er, Yb is a two stage process for all three mentioned bands; the log-to-log slope of UCL dependence on the pump power is 1.5 for red band and 1.9 for yellow and green bands.

Acknowledgement

The authors are grateful to D. L. Chertkova for excellent technical assistance. The work was partially supported by the Russian Foundation for Basic Research Grant 15-52-53080, by the Russian President Grant SS-7612.2016.2, and by Project №0358-2015-0012 of SB RAS Program №II.2P.

References

- [1] W. Lenth, R.M. Macfarlane, Upconversion lasers, *Opt. Photonics News* 3 (1992) 8.
- [2] R.P. Rao, Tm³⁺ activated lanthanum phosphate: a blue PDP phosphor, *J. Lumin.* 113 (2005) 271–278.
- [3] F. Wang, R.R. Deng, J. Wang, Q. Wang, Y. Han, H. Zhu, X. Chen, X. Liu, Tuning upconversion through energy migration in core-shell nanoparticles, *Nat. Mater.* 10 (2011) 968–973.
- [4] K. Kuningsas, T. Rantanen, U. Karhunen, T. Lovgren, T. Soukka, Simultaneous use of time-resolved fluorescence and anti-stokes photoluminescence in bioaffinity assay, *Anal. Chem.* 77 (2005) 2826–2834.
- [5] T. Soukka, K. Kuningsas, T. Rantanen, V. Haaslahti, T. Lovgren, Photochemical characterization of up-converting inorganic lanthanide phosphors as potential labels, *J. Fluoresc.* 15 (2005) 513–528.
- [6] L. Shi, C. Li, Q. Shen, Z. Qiu, White upconversion emission in Er³⁺/Yb³⁺/Tm³⁺-codoped LiTaO₃ polycrystals, *J. Alloys Compd.* 591 (2014) 105–109.
- [7] E.A. Ferreira, F.C. Cassanjes, G. Poirier, Crystallization behavior of a barium titanate tellurite glass doped with Eu³⁺ and Er³⁺, *Opt. Mater.* 35 (2013) 1141–1145.
- [8] K. Teshima, S. Lee, N. Shikine, T. Wakabayashi, K. Yubuta, T. Shishido, S. Oishi, Flux growth of highly crystalline NaYF₄:Ln (Ln=Yb, Er, Tm) crystals with upconversion fluorescence, *Cryst. Growth Des.* 11 (2011) 995–999.
- [9] A. Shalav, B.S. Richards, M.A. Green, Luminescent layers for enhanced silicon solar cell performance: up-conversion, *Sol. Energy Mater. Sol. Cells* 91 (2007) 829–842.
- [10] X. Li, D. Zhao, F. Zhang, Multifunctional upconversion-magnetic hybrid nanostructured materials: synthesis and bioapplications, *Theranostics* 3 (2013) 292–305.
- [11] C.S. Lim, A.S. Aleksandrovsky, M.S. Molokeev, A.S. Oreshonkov, V.V. Atuchin, Microwave sol-gel synthesis and upconversion photoluminescence properties of CaGd₂(WO₄)₄:Er³⁺/Yb³⁺ phosphors with incommensurately modulated structure, *J. Solid State Chem.* 228 (2015) 160–166.
- [12] C.S. Lim, A.S. Aleksandrovsky, M.S. Molokeev, A.S. Oreshonkov, V.V. Atuchin, The modulated structure and frequency upconversion of CaLa₂(MoO₄)₄:Ho³⁺/Yb³⁺ phosphors prepared by microwave synthesis, *Phys. Chem. Chem. Phys.* 17 (2015) 19278–19287.
- [13] C.S. Lim, V.V. Atuchin, A.S. Aleksandrovsky, M.S. Molokeev, A.S. Oreshonkov, Microwave sol-gel synthesis of CaGd₂(MoO₄)₄:Er³⁺/Yb³⁺ phosphors and their upconversion photoluminescence properties, *J. Am. Ceram. Soc.* 98 (2015) 3223–3230.
- [14] A.S. Aleksandrovsky, I.A. Gudim, A.S. Krylov, A.V. Malakhovskii, V.L. Temerov, Upconversion luminescence of YAl₃(BO₃)₄:Yb³⁺, Tm³⁺ crystals, *J. Alloys Compd.* 496 (2010) L18–L21.
- [15] J.F. Suyver, J. Grimm, K.W. Krämer, H.U. Güdel, Highly efficient near-infrared to visible up-conversion process in NaYF₄:Er³⁺, Yb³⁺, *J. Lumin.* 114 (2005) 53–59.
- [16] M. Banski, A. Podhorodecki, J. Misiewicz, NaYF₄nanocrystals with TOPO ligands: synthesis-dependant structural and luminescent properties, *Phys. Chem. Chem. Phys.* 15 (2013) 19232–19241.
- [17] A. Aebscher, M. Hostettler, J. Hauser, K. Krämer, T. Weber, H.U. Güdel, H.-B. Bürgi, Structural and spectroscopic characterization of active sites in a family of light-emitted sodium lanthanide tetrafluorides, *Angew. Chem. Int. Ed.* 45 (2006) 2802–2806.
- [18] S. Hao, L. Sun, G. Chen, H. Qiu, C. Xu, T.N. Soitah, Y. Sun, C. Yang, Synthesis of monoclinic Na₃ScF₆:1 mol% Er³⁺/2 mol% Yb³⁺ microcrystals by a facile hydrothermal approach, *J. Alloys Compd.* 522 (2012) 74–77.
- [19] X. Teng, Y. Zhu, W. Wei, S. Wang, J. Huang, R. Naccache, W. Hu, A.I.Y. Tok, Y. Han, Q. Zhang, Q. Fan, W. Huang, J.A. Capobianco, L. Huang, Lanthanide-doped Na₃ScF_{3-x}Nanocrystals: crystal structure evolution and multicolor tuning, *J. Am. Chem. Soc.* 134 (2012) 8340–8343.
- [20] H. Fu, G. Yang, S. Gai, N. Niu, F. He, J. Xu, P. Yang, Color-tunable and enhanced luminescence of well-defined sodium scandium fluoride nanocrystals, *Dalton Trans.* 42 (2013) 7863–7870.
- [21] X. He, B. Yan, A novel Sc³⁺-containing fluoride host material for down- and up-conversionluminescence, *J. Mater. Chem. C* 1 (2013) 3910–3912.
- [22] X. He, B. Yan, Novel series of quaternary fluoride nanocrystals: room-temperature synthesis and down-shifting/up-converting multicolor fluorescence, *J. Mater. Chem. C* 2 (2013) 2368.
- [23] J. Castaneda, M.A. Meneses-Nava, O. Barbosa-Garcia, E. de la Rosa-Cruz, J.E. Mosino, The red emission in two and three steps up-conversion process in a doped erbium SiO₂-TiO₂ sol-gel powder, *J. Lumin.* 102–103 (2003) 504–509.
- [24] S. Obregon, G. Colon, Evidence of upconversion luminescence contribution to the improved photoactivity of erbium doped TiO₂ systems, *Chem. Commun.* 48 (2012) 7865–7867.
- [25] P.A. Loiko, N.M. Khaidukov, J. Mendez-Ramos, E.V. Vilejshikova, N.A. Skoptsov, K.V. Yumashev, Up- and down-conversion emissions from Er³⁺ doped K₂YF₅ and K₂YbF₅, *J. Lumin.* 170 (2016) 1–7.
- [26] M. Rico, M.C. Pujol, F. Diaz, C. Zaldo, Effects of sample orientation and erbium concentration, *Appl. Phys. B* 72 (2001) 157–162.
- [27] F. Vetrone, J.-C. Boyer, J.A. Capobianco, A. Speghini, M. Bettinelli, 980 nm excited upconversion in an Er-doped ZnO-TeO₂ glass, *Appl. Phys. Lett.* 80 (2002) 1752–1754.
- [28] A.S. Krylov, M.S. Molokeev, S.V. Misul, I.N. Safonov, S.N. Krylova,

- A.S. Oreshonkov, A.A. Ivanenko, V.A. Zykova, Yu I. Ivanov, A.A. Sukhovsky, V.N. Voronov, A.N. Vtyurin, Crystal structure and phase transitions of layered perovskite-like CsScF_4 crystal, Crys. Eng. Comm. (2016), <http://dx.doi.org/10.1039/C6CE01144F>.
- [29] Bruker AXS TOPAS V4: General Profile and Structure Analysis Software for Powder Diffraction Data. – User's Manual, Bruker AXS, Karlsruhe, Germany, 2008.
- [30] R.D. Shannon, Revised effective ionic radii and systematic studies of interatomic distances in halides and chalcogenides, Acta Cryst. A 32 (5) (1976) 751–767.
- [31] A.V. Malakhovskii, A.L. Sukhachev, S.L. Gnatchenko, I.S. Kachur, V.G. Piryatinskaya, V.L. Temerov, A.S. Krylov, I.S. Edelman, Spectroscopic properties and energy levels of Yb^{3+} ion in huntite structure, J. Alloys Compd. 476 (2009) 64–69.
- [32] M.F. Reid, P.A. Tanner, Electronic spectra of $\text{Cs}_2\text{NaYbF}_6$ and crystal field analyses of YbX_6^{3-} ($\text{X}=\text{F}, \text{Cl}, \text{Br}$), J. Phys. Chem. 110 (2006) 14939–14942.
- [33] M. Pollnau, D.R. Gamelin, S.R. Lüthi, H.U. Güdel, Power dependence of upconversion luminescence in lanthanide and transition-metal ion system, Phys. Rev. B 61 (2000) 3337–3346.